Int. Journ. of Peening Science and Technology, Vol. 1, pp. 137–154
Reprints available directly from the publisher
Photocopying permitted by license only

Laser Shock Peening of Orthopaedic Ti-6Al-7Nb: Evaluation of Topography, Wetting Characteristics, Microstructure and Residual Stress

X. SHEN[1*], P. SHUKLA[1], F. YAO[2], S. NATH[1], Z. AN[3] AND J. LAWRENCE[1]

[1]*Coventry University, School of Mechanical, Aerospace and Automotive Engineering, Faculty of Engineering, Environment and Computing, Priory Street, Coventry, CV1 5FB, United Kingdom*
[2]*The No.1 Department of orthopaedic Surgery, The No.1 People's Hospital of JiaShan, China*
[3]*Science and Technology on Plasma Dynamics Laboratory, Air Force Engineering University, China*

This paper is focused on a study of wetting characteristics post laser shock peening (LSP) of orthopaedic titanium alloy (Ti-6Al-7Nb) for the first-time. A 10J, 8ns, 1064nm wavelength, Nd:YAG Laser was employed. Residual stress was measured using the incremental hole drilling method. Residual stress results showed maximum compressive stress of -420 MPa, and -100 MPa at a depth of 0.8mm. The surface roughness was increased from 0.15 μm to 0.87 μm after multiple LSP impacts. The contact angle measurements were undertaken by using a sessile drop device with water and ethylene glycol. Both liquids showed that LSP increase the contact angle by 17% and 30.4% respectively using water and ethylene glycol. In addition, further verification was made using the Fowkes model to calculate the surface energy. This yielded the total energy, diversion and polar component to have reduced. The increased contact angle of LSPned samples were affected by combination of increased surface roughness and decreased surface energy. The findings in this study not only form a base for further research, but also reveal the possibility of strengthening titanium implants and rendering them to become more biocompatible.

Keywords: *LSP, wettability, contact angle, Ti-674-Nb, residual stress, SEM, 3-D profiling*

Corresponding author's e-mail: s673864902@126.com

1 INTRODUCTION

Laser shock peening (LSP) has been successfully applied in aeronautic and auto industry over the last two decades. Over the years, researchers have dedicated time to improve the mechanical properties of metallic materials such as fatigue life, wear, and corrosion resistance using LSP. Recently, researchers are also investigating the effect of laser shock peening in another area. In particular, the biological properties of orthopaedic implants, especially the wettability. The wettability of orthopaedic implants is one of the most determining factors in efficiently governing osteogenic activity, involving adhesion, proliferation and differentiation of osteoblasts cells. For the majority of implant materials, wettability is fixed [1-5]. How to change the wetting characteristics in order to improve the biocompatibility of implants without changing surface chemical components has become a new research focus.

Some researchers have already started to do some researches about the effects of LSP on contact angles of metals. Specifically, Vinodh *et al.* [6-7] analysed the effect of LSP on the dynamic corrosion rate of magnesium. As one important property, wettability was also determined and the contact angles of peened samples were increased by 66%. Moreover, Prabhakaran *et al.* [8], employed low energy laser shock peening without coating (LSPwC) to measure the wettability of AISI 304 austenitic stainless steel and found that the hydrophilic unpeened surface was converted into the hydrophobic surface. The contact angle of AISI 304 austenitic stainless steel was significantly increased from 34.24° to 95.75°. Currently, as the dominant material used for implants fabrication, the effect of LSP on the wettability of titanium has not been investigated to-date.

Thus, the focus of this paper was to deploy LSP to change the contact angle of titanium implants for the first-time, since LSP has the capability to change the surface roughness and surface energy, while avoiding the introduction of new chemical substances. Moreover, a Ti-6Al-7Nb titanium alloy was employed due to its excellent biocompatibility and mechanical properties compared Ti-6AL-4V. It is also known that vanadium (V) would be released into the body environment when the surface oxide layer is broken, causing ion toxicosis [9]. Nevertheless, in Ti-Al-67-Nb, niobium (Nb) does not have such a problem. Thus, Ti-6Al-7Nb has more advantage than the most widely used Ti-6Al-4V alloy. However, with orthopaedic implants materials in general, processing stable mechanical properties is necessary, with excellent biocompatibility is also being mandatory. As discussed in previous literatures, LSP can greatly improve the mechanical properties of metal materials. But if this technique needs to be used for implant applications, then the biocompatible aspect of it should be considered too. Our previous findings showed that improvement of wear resistance in Ti-6Al-7Nb alloy subjected to LSP [10] can be achieved. Adding to that, this study has formed a

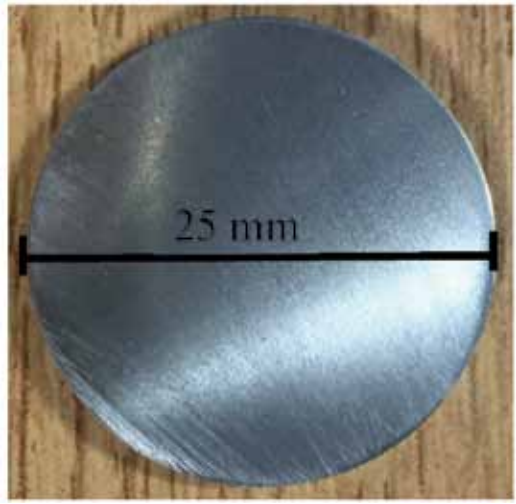

FIGURE 1
An optical image of Ti-6Al-7Nb alloy experimental sample.

TABLE 1
Elemental analysis of Ti-6Al-7Nb alloy (Astm F1295 Rev 11).

Element	Al	Nb	Ta	Fe	N	O	C	H2	Ti
Wt.%	6.1	6.88	0.5	0.19	0.008	0.166	0.04	0.002	Bal

future research stream for strengthening and rendering titanium implants to becoming more biocompatible.

2 MATERIAL AND METHODS

2.1 Details of Ti-6Al-7Nb alloy and sample preparation

Ti-6Al-7Nb samples (show in Figure 1 with its elemental composition in Table 1) were cut into φ25mm x8mm, grinded from 300μm to 1200μm grit size, SiC abrasive paper in stages until the material comprised of Sa (arithmetic mean height) 0.15 μm surface finish. Two samples were used for the laser LSP experiments and one for the analysis on the untreated areas. The etching reagent was 100ml beaker in 20ml Kroll's reagent in which the samples were immersed to reveal surface integrity. Samples were then prepared to the size 10mm × 10mm using wire electro-discharge machining and then immersed in etching solution for 20 seconds then washed in deionized water, dried in the fume hood for the microstructural analysis.

TABLE 2
Laser shock peening parameters employed for the surface treatment of Ti-6Al-7Nb.

Parameters	**Value**
Pulse energy (J)	6.5
Laser wavelength (nm)	1064
Spot diameter (mm)	3
Radiance Density ($W/mm^2/Sr^{-1}/\mu m$) [11-13]	2.52
Number of laser impacts	1
Overlapping rate (%)	50
Pulse duration (ns)	8
Divergence (mrad)	0.5
Pulse Repetition Rate (Hz)	5

2.2 Laser shock processing method

The LSP experiments were conducted by a Q-Switched Nd:YAG laser (LPY10J; Litron, Rugby, UK), using a wavelength of 1064nm and 8ns pulse width. The laser comprised of a flat-top beam and a M^2 value of 1.99 with a beam divergence of 0.5 mrad. The pulse energy was 6.5J per pulse with a spot diameter was 3 mm focused using a fused silica lens of 50mm diameter. This resulted to a power density of $11.5GW/cm^2$ and a shock pulse pressure of 5.77 GPa in Table.2. The LSP experiment overlap was 50% with 3 impacts according to the one peening sequence presented in Figure 2(b). The water layer was used as the confinement layer, while coating absorb layer was black tape. Figure 2 (a) presents a schematic diagram of the process and (b) shows one pulse overlapping sequence employed.

2.3 Measurements and characterization

2.3.1 Surface Roughness

A 3-D profiler (Contour GT-K, Bruker, Germany.) was employed to measure surface roughness of the Ti-6Al-7Nb alloy before and after LSP. The scanned area for surface roughness determination was 5×5 mm^2 and was measured x5 to ensure the surface roughness values were the same and consistent.

2.3.2 Incremental Residual Stress

The cross-section residual stress was tested by using the incremental hole drilling method with a system developed by Stresscraft, UK. The strain relaxation was measured by wired gauges in a standard three-gauge rosette (two gauges at 90° with a third at 45°). The holes were incremen-

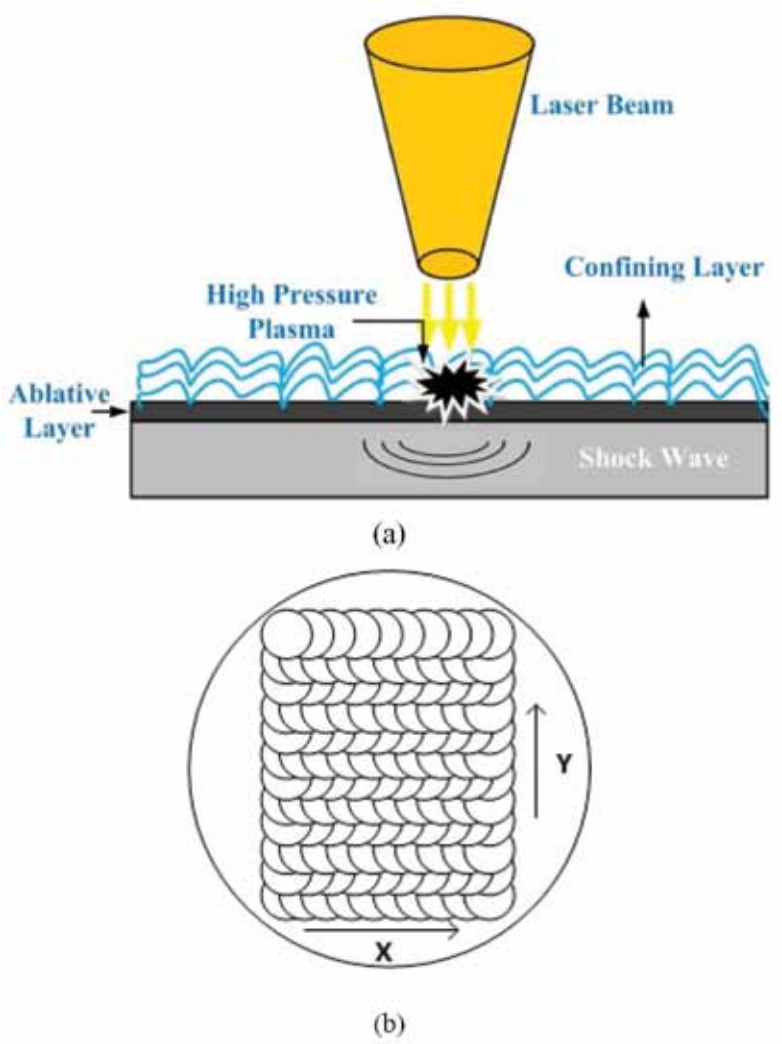

FIGURE 2
A schematic diagram of the laser shock peening process in (a); and (b) the pulse overlapping sequence employed for the laser shock peening surface treatment of Ti-6Al-7Nb [10].

tally drilled with a diameter of 2mm and a maximum depth of 1mm. The relaxed strains were recorded at 13 different increments. Four increments were of 32 μm, and further four increments were of 64 μm. Additional 8 increments were of 128 μm, to a total hole depth of nearly 1 mm. The data were interpreted by Stresscraft RS INT software. Young`s modulus of 105 GPa and Poission`s ration of 0.36 were the input properties in order to calculate the residual stresses.

2.3.3 Wettability

The surface wettability characteristic was measured by using goniometry instrument (DAS 100, DAS, Germany) at room temperature (20°C). The droplet volume of 250 μl and was separately filled with distilled water and ethylene glycol. Each time, 5μl testing liquid was dropped on the surface of the samples. The goniometer calculated the contact angle thereafter, with a processing time of 10 secs. Five sets of contact angles were measured for each sample at different locations to validate the consistency of the data.

3 RESULTS AND DISCUSSION

3.1 Microstructure observation of Ti-6Al-7Nb

The grain refinement has significant relationship with the mechanical properties of the metal alloys. Figure 3 shows the optical cross-section of Ti-6Al-7Nb alloy before and after LSP. From both images coarse grains are distributed non-uniformly over the cross-section. According to grain intercept method, the coarse grains of as-received sample was 6.25 μm, while that of LSPned sample was 3.71 μm. Therefore, the refinement percentage of coarse grain is 68%.

SEM was also used to evaluate the microstructure of the Ti-6Al-7Nb alloy. Figure 4 presents the SEM observations of the untreated and the surface after LSP. As shown in Figure 4, the original microstructure of Ti-6Al-7Nb alloy consists of globular and acicular α and residual β [14 - 17]. The acicular and globular α distribute non-uniformly that the grains are coarse-grains and have clear phase boundaries. Inside the coarse α-grains, there are lots of fine α-rains which possess different grain orientations as shown in Figure 4(b). The grain boundaries between the fine α-grains are clear. The average fine grain size of as-received samples is 266.6 nm. Having said that, the grains decreased after LSP to 150 nm which is about 78% reduction and is exceptional reduction indicating a strengthen surface.

3.2 Surface roughness

Figure 5 show the 3-D topography of Ti-6Al-7Nb alloy before and after LSP. The untreated samples were polished from 300μm to 1200μm grit size, SiC abrasive paper in stages. Moreover, it can be seen that scratch distributed non-uniformly on the untreated samples. In Figure 5(b) the scratches are non-existent after LSP, particularly in the treated areas, and more micro-grooves and dimples were presented on the surface due to the high-pressure waves from the process generating the dimpling effect that you see with shot peening in general. With that said the roughness after LSP increases from 0.194μm to 0.445μm as shown in In Table 3.

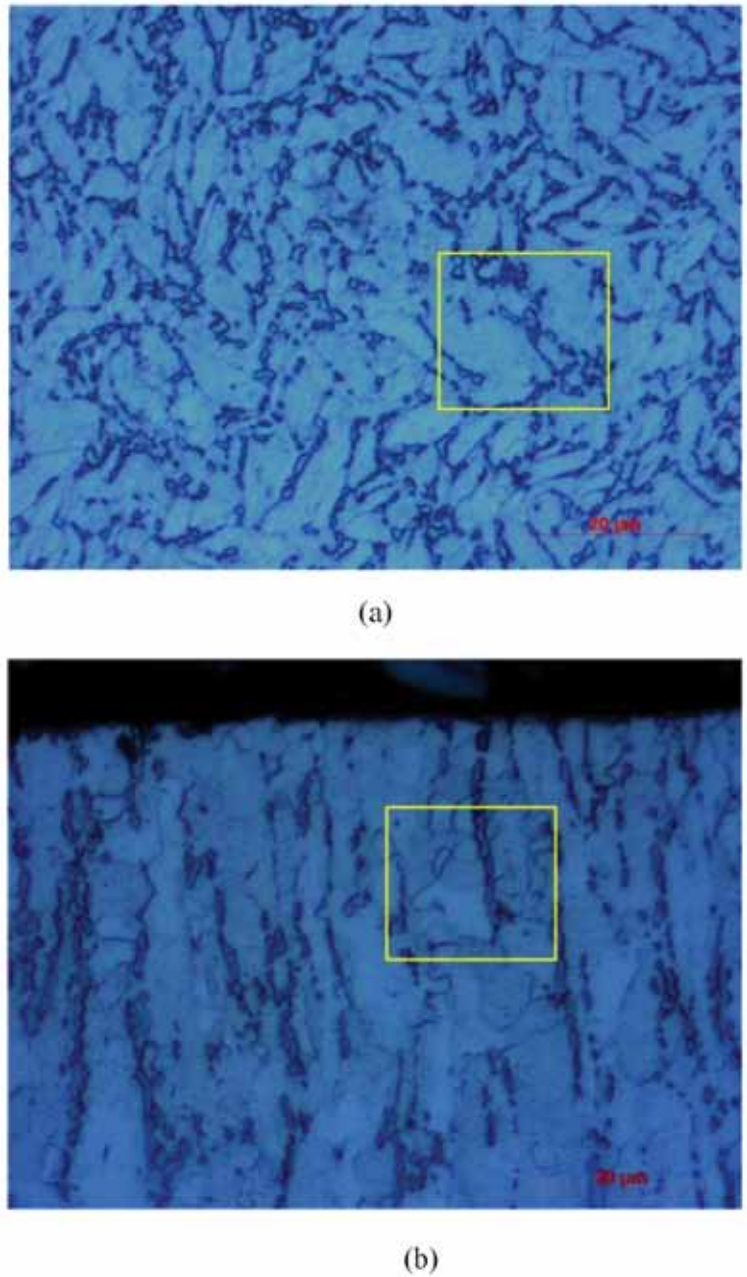

FIGURE 3
Optical image showing the cross-section of the as-received and laser impacted surface of the Ti-6Al-7Nb in (a); and laser shock peened surface in (b).

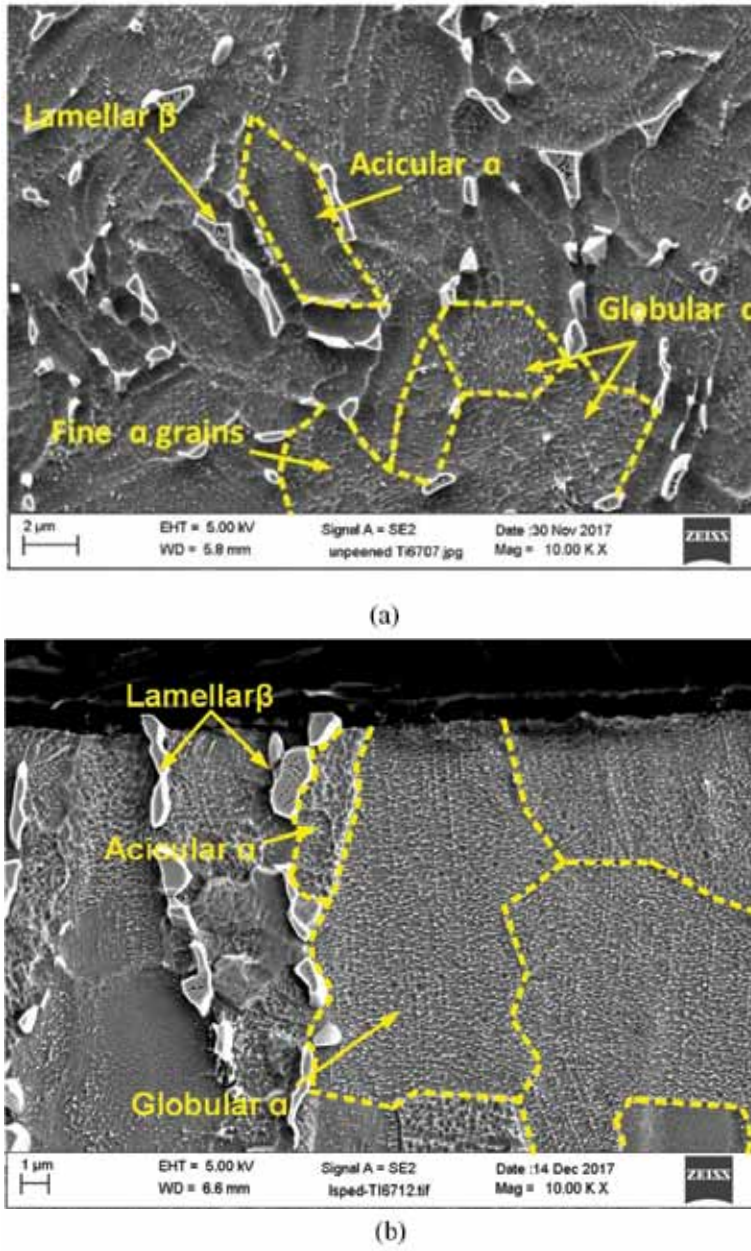

FIGURE 4
SEM image showing the microstructure of the Ti-6Al-7Nb, before and after laser shock peening in both (a) and (b).

What is more, Figure 6(a) and (b) shows the 2-D profile of the unpeened and LSPned Ti-6Al-7Nb alloy. Figure 6(c) and (f) shows cross-sectional 2-D surface

TABLE 3
Surface roughness of Ti-6Al-7Nb in 3-D.

	Sa	Sp	Sq	Ssk	Sv	Sz
Untreated	0.193.8	5.246	0.252	-0.69	-5.59	10.835
LSPend	0.445	2.596	0.576	-3.78	-12.9	15.47

TABLE 4
A 2-D profile height of Ti-6Al-7Nb.

	Ra	Rp	Rq	Rt	Rv
Untreated	0.194	5.246	0.253	10.838	-5.589
LSPed	0.446	2.596	0.578	15.479	-12.883

roughness form X-and-Y axis of the unpeened and LSPned samples. The surface height of the untreated sample scattered from a peak of 0.5μm to a depth of -0.5μm in both X and Y directions. But after LSP, the surface roughness scattered from -1.0μm to -1.5μm in X and ranged from 1.0μm to -1.0μm. As shown in table 4, the average roughness Ra is increased from 0.194μm (unpeened sample) to 0.446μm (peened sample). According to above surface roughness data, the by-product created by LSP which is the surface roughness, could in turn contributes to the changes to the contact angles as the increase in the surface roughness takes place.

3.3 Residual stress

Laser shock peening can introduce a stable compressive residual stress layer on the surface of metallic materials through high pressure shock wave [10]. As shown in Figure 7, the distribution of cross-sectional residual stress before and after LSP resulted to a stable compressive residual stress layer at a depth of 800 μm. Surface residual stress of as-received samples is -60 MPa caused by surface finishing. Onwards along the depth, residual stress varies from 0 MPa to 60 MPa. Surface residual stress of impacted samples was -250MPa. This was around x5 than that of the as-received. Additionally, compressive residual stress is at the highest at a depth of 80 μm, thereby, starting to decrease along the depth to stable value as the intensity of the pressure waves decrease.

3.4 Wettability characteristics

Wetting characteristics have great influence on osseointegration. As a direct parameter reflecting the wetting characteristics of the sample, contact angle θ is affected by many factors including surface roughness and surface energy. Shown from previous work, Caralapatti [7] and Prabhakaran *et al.* [8] found the phenomenon that contact angle θ was increased after laser peened.

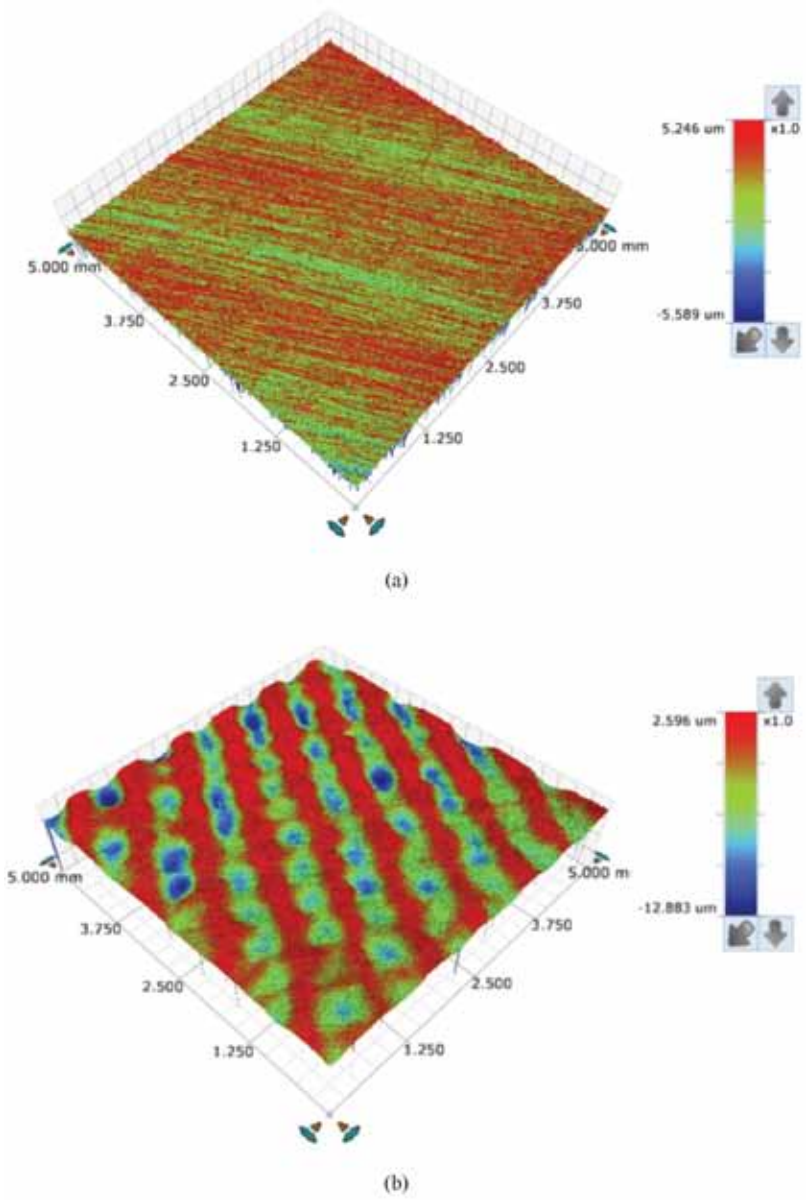

FIGURE 5
A 3D surface map showing the topography of Ti-6Al-7Nb prior-to laser shock peening in (a) and after laser shock peening in (b).

The typical Wendzel model [18, 19] is shown in Figure 7 and equation (1):

$$\cos\theta^{*} = r(\gamma_{SG} - \gamma_{SL}) / \gamma_{LG} \tag{1}$$

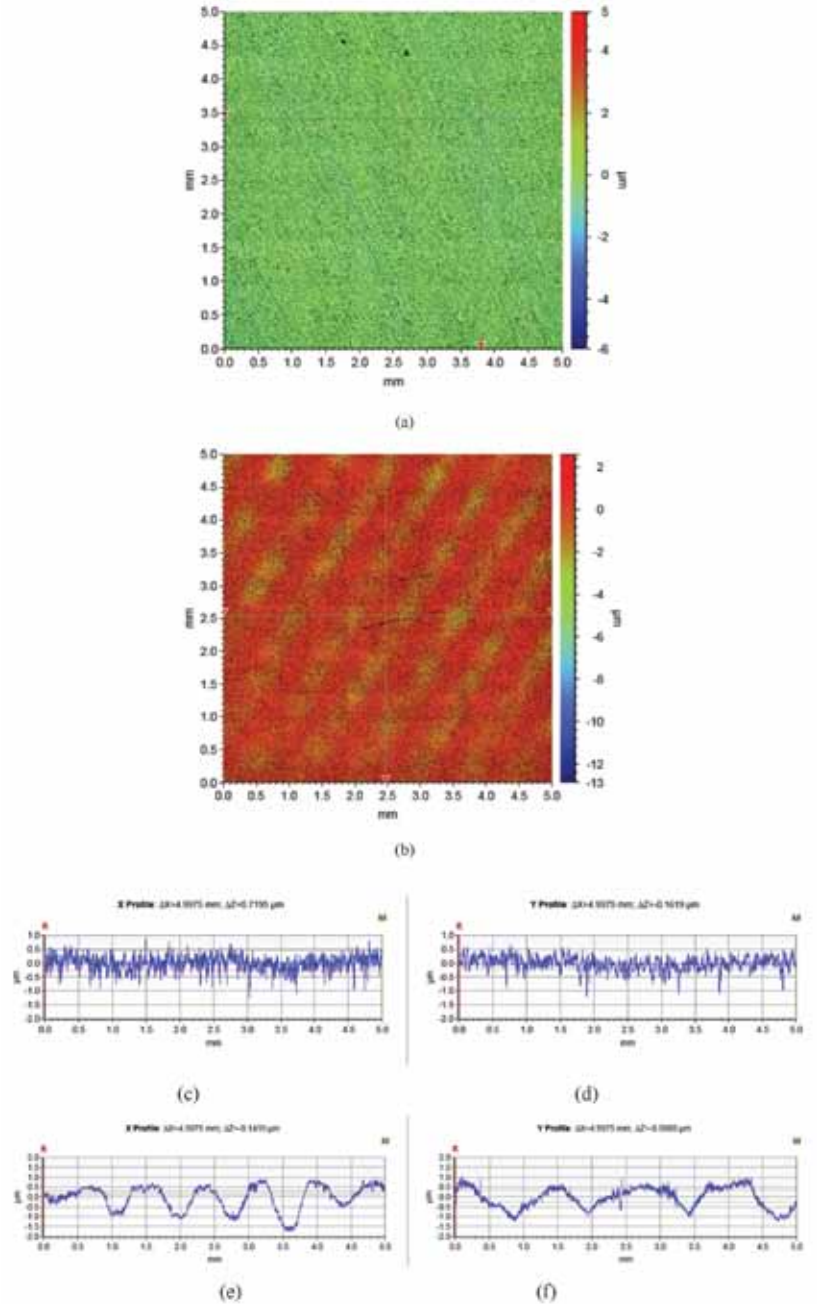

FIGURE 6
A 2-D surface topography of Ti-6Al-7Nb alloy.

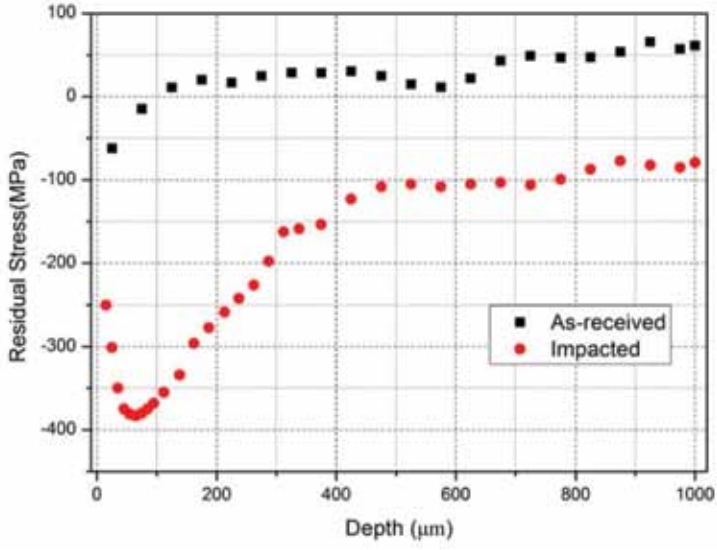

FIGURE 7
A cross-sectional distribution of residual stress of Ti-6Al-7Nb before and after laser shock peening.

Where, $\cos\theta^*$ is the real contact angle; r is surface roughness factor; γ_{SG} is the tension between solid and gas; γ_{SL} is the tension between solid and liquid; γ_{LG} is the tension between liquid and gas.

Therefore, it is necessary to calculate another factor which is the surface energy which can change the difference of contact angle. Fowkes [20 - 21], assumed that surface free energy of solid is a sum of independent components, associated with specific interactions:

$$\gamma_{SG} = \gamma_{SG}^{d} + \gamma_{SG}^{p} + \gamma_{SG}^{h} + \gamma_{SG}^{i} + \gamma_{SG}^{ab} + \gamma_{S}^{o} \tag{2}$$

Where, γ_{SG} is surface free energy of a solid; γ_{SG}, γ_{SG}, γ_{SG}, γ_{SG}, γ_{SG}^{o} are the dispersion, polar, hydrogen, induction and acid-base components, and γ_{SG} is all remaining interactions. Combined with young equation (3), Fowkes suggested equation (4), which used 2 components to calculate solid surface energy.

$$\gamma_{SG} = \gamma_{SL} + \gamma_{LG}\cos\theta \tag{3}$$

$$\frac{\gamma_{lg}(1+\cos\theta)}{2} = \sqrt{\gamma_{sg}^{d}\gamma_{lg}^{d}} + \sqrt{\gamma_{sg}^{p}\gamma_{lg}^{p}} \tag{4}$$

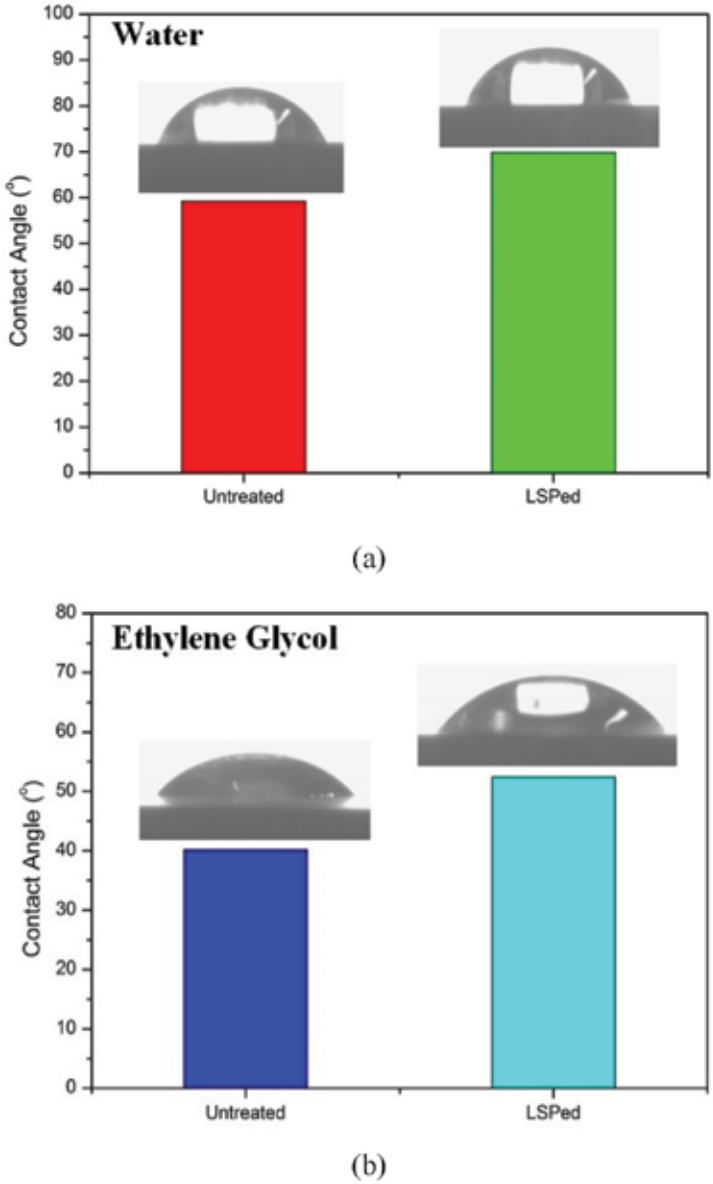

FIGURE 8
Contact angle images of Ti-6Al-7Nb with (a) water and (b) ethylene glycol.

Where, θ refers to the contact angle; In equation (4), only γ_{sg}, γ_{sg}, are unknown. Thus, using two reference liquid which have γ_{lg}^{d}, γ_{lg}^{p} and γ_{1g} calculate γ_{sg} and γ_{sg}. We used distilled water (γ^{P}= 51.0 mD/m, γ^{D}=21.8 mN/m, γ^{T}=72.8 mN/m) and ethylene glycol (γ^{P}= 19 mD/m, γ^{D}=29 mN/m,

TABLE 5
Wetting characteristic of Ti-6Al-7Nb alloy before and after laser shock peening.

	Liquid	Ra	Sa	γ^D	γ^P	γ^T	Contact angle θ
Untreated	Water	0.15	0.149	42.891	9.864	52.754	59.19
	Ethylene glycol						40.184
LSPed	Water	0.875	0.873	30.326	4.248	34.574	69.818
	Ethylene glycol						52..41

γ^T=48 Mn/m) to calculate the total surface energy including polar component and diverse component. The results are shown in Table 5 and Figure 8.

The results of contact measurements indicate that contact angles are increased by using both liquids. As shown in Table 5 and Figure 8, the contact angle increased from 59.19° to 69.818° with water liquid, and 40.18° to 52.41° with ethylene glycol.

If the valleys of a coarse surface were filled by liquid such as water, then the Wenzel`s model is more suitable. Normally, according to Wenzel Model shown in Figure 8, the contact angle of the LSPned samples should decrease while surface roughness of samples increased. But the contrast result is that contact angle was increased. Thus, Cassie-Baxter model, shown in Figure 9, or mixed regime of both [22 - 24] may be used in this case. The explanation of Cassie-Baxter model suggested that the fluid adhering onto the top of the protrusions would create a pocket of air underneath [25].

The reason why contact angle was increased was because the γ^P, γ^D and γ^T in both liquids were all decreased. High surface energy can lead to low hydrophilicity which meant that low contact angle resulted. Thus, the decreased in surface energy, combined with increased surface roughness increased the contact angle.

Additionally, due to the ablation of LSP, the contaminations, namely; dirt was removed, which contribute to improving the surface free energy [26]. Since the surface free energy of contaminations were low, the removal of contaminations can increasing the surface energy thereby contributing to the biological properties of implants. It is said that contact angle of 70° [27] is considered to be ideal for cell attachment and better bonding with osteoblast which is key for cell adhesion. When implants are serving inside the human body, they undergo different interactions such as cells, proteins and adhesion. What is more important, osteointegration was also influence by surface wettability of implants. However, the effect of LSP on cell adhesion and osteointegration of medical-grade metals have not been investigated.

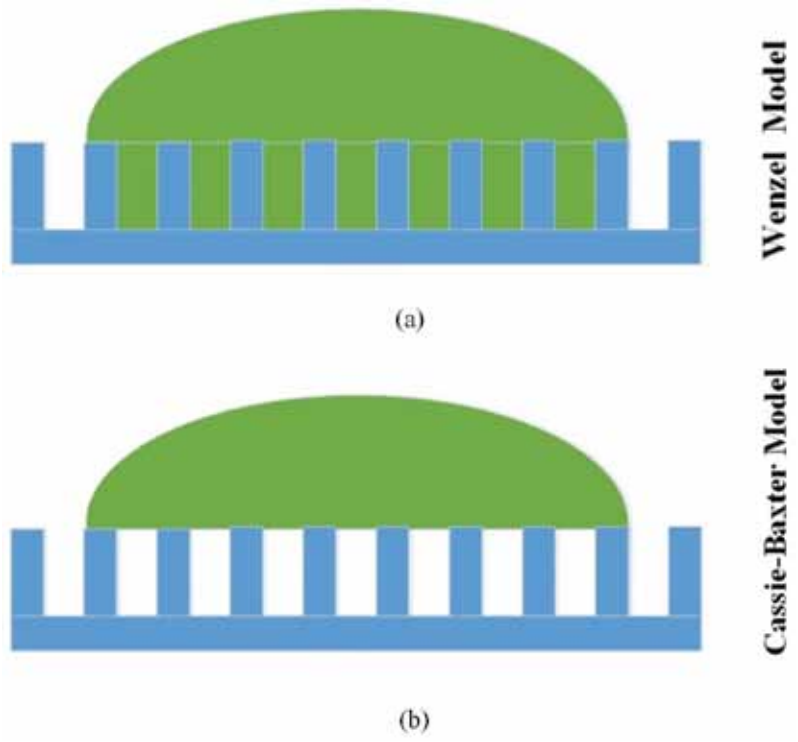

FIGURE 9
The schematic diagrams of (a) Wenzel model and (b) Cassie-Baxter model.

4 CONCLUSIONS

It is very important to provide a strengthening mechanism for implant metals due to the obvious failures resulting to significant damage and loss of patient's time, money and the potential pain *via* repetitive surgeries. Therefore, it proves very useful to investigate the biological effect of LSP strengthening technique on medical-grade metallic materials such as titanium alloys. Thus, the focus of this paper is on the topography, wetting characteristics, microstructure and residual stress which were investigated for the first-time prior-to and post laser shock peening of orthopaedic grade Ti-6Al-7Nb. The wide range of analysis verified and rendered the following conclusions:

1) Three LSP impacts increase the surface roughness by 127%.
2) In the cross-section, the coarse grain size was decreased from 6.25μm to 3.71 μm, while the refinement of fine grain size was from 266.5nm to 150nm.

3) LSP increased the contact angle from 59.19° to 69.81° by using water and 40.18° to 52.41° by Ethylene glycol as result of the decreased surface energy and increased surface roughness.

NOMENCLATURE

Ra	Arithmetical mean roughness value over the entire measured length (μm)
Rp	Maximum profile peak height/ valley depth are the distance from the mean line (μm)
Rq	Average between the height deviations and the mean line (μm)
Rt	Total height of the roughness profile over the length (μm)
Rv	Surface to the highest/lowest point along the sample length (μm)
Sa	The arithmetic mean of the absolute values of the surface departures from the mean plane (μm)
Sp	The height of the highest peak within the defined area (μm)
Sq	The root mean square value of the ordinate values within the definition area (μm)
Ssk	Asymmetry of the profile about the mean plane (μm)
Sv	The absolute value of the height of the largest pit within the defined area (μm)
Sz	The sum of the largest peak height value and the largest pit depth within the area (μm)

Greek Symbols

γ_{sg}	The tension between solid and gas
γ_{SL}	The tension between solid and liquid
γ_{LG}	The tension between liquid and gas
γ_{SG}^{d}	Dispersion component
γ_{SG}^{p}	Polar component
γ_{SG}^{h}	Hydrogen component
γ_{SG}^{i}	Induction component
γ_{SG}^{ab}	Acid-base component
γ^{P}	Polar energy
γ^{D}	Dispersion energy
γ^{T}	Total surface energy

5 ACKNOWLEDGEMENT

This work was supported by the Engineering Physical Sciences Research Council's (EPSRC) laser loan pool scheme run by the Science & Technology Facilities Council (STFC) with the Grant no: EP/G03088X/1, (13250017 – NSL4)).

REFERENCES

[1] Chen, D., Gao, M., Fu, Y., Xu, X., Hao, Z. A facile approach to manipulation of osteogenic activity of orthopaedic implants by in situ electrically controlled wettability. *Electrochimica Acta* **182** (2015), 841-846.

[2] Padial-Molina, M., Galindo-Moreno, P., Fernandez-Barbero, J. E., O`Valle, F., Jodar-Reyes, A. B., Ortega-Vinuesa, J. L., Ramon-Torregrosa, P. J. Role of Wettability and nanoroughness on interactions between osteoblast and modified silicon surfaces. *Acta Biomaterialia* **7** (2015), 771-778.

[3] Rosales-Leal, J.I., Rodriguesz-Valverde, M. A., Mazzaglia, G., Ramon-Torregrosa, P. J., Diaz-Rodriguez, L., Garcia-Martinez, O., Vallecillo-Capilla, M., Ruiz, C., Cabrerizo-Vilchez, M. A. Effect of roughness, wettability and morphology of engineered titanium surfaces on osteoblast-like cell adhesion. *Colloids and Surfaces A: Physicochemical and Engineering Aspects*, **365** (2011), 222-229.

[4] Kulkarni, M., Patil-Sen, Y., Junkar, I., Kulkarni, C.V., Loreenzetti, M., Iglic A. Wettabiltiy Studies of Topologically distinct titanium surfaces. *Colloids and Surfaces B: Biointerfaces*, **129** (2015), 47-53.

[5] Hotchkiss, K.M., Reddy, F.B., Hyzy, S.L., Schwartz, Z., Boyan, B.D., Olivares-Navarrete, R. Titanium surface characteristics, including topography and wettability after macrophage activation. *Acta Biomaterialia* **31** (2016), 425-434.

[6] Caralapatti, V.C., Narayanswamy, S. Analyzing the effect of high repetition laser shock peening on dynamic corrosion rate of magnesium. *Optics and laser Technology* **93** (2017), 165-174.

[7] Caralapatti, V.C., Narayanswamy, S. Effect of high repetition laser shock peening on biocompatibility and corrosion resistance of magnesium. *Optics & Laser Technology* **88** (2017), 75-84.

[8] Prabhakaran, S., Aniket K., G. Vasanth, Kalainathan, S., Shukla P., Vasudevan V. K. Laser shock peening without coating induced residual stress distribution, wettability characteristics and enhance pitting corrosion resistance of austenitic stainless steel. *Applied Surface Science* **428** (2018), 17-30.

[9] Semlitsch, M.F., Weber, H., Streicher, R.M., Schön, R. Joint replacement components made of hot-forged and surface-treated Ti–6Al–7Nb alloy. *Biomaterials* **13** (1992), 781-788.

[10] Shen, X., Shukla. P., Nath, S., Lawrence, J. Improvement in mechanical properties of titanium alloy (Ti-6Al-7Nb) subject to multiple laser shock peening. *Surface and Coatings Technology* **327** (2017), 101-109.

[11] Shukla, P.P., Lawrence, J. Role of laser beam radiance in different ceramic processing: A two wavelength comparison. *Optics and Laser Technology* **54** (2013), 380-388.

[12] Shukla, P., Lawrence J., Zhang, Yu. Understanding Laser-beam brightness: A Review on a New Prospective in Materials Processing', *Optics and Lasers in Engineering* **75** (2015), 40-51.

[13] Shukla, P.P., and Lawrence, J. Identification of Optical Parameters for Determination of Radiance, *Journal of Optics*, Optical Society of India **44** (2015), 12-19.

[14] Oliveira, D.P., Prokoiev, E., Sanches, L.F.R., Valiev, R.Z., Botta, W.J., Junior, A.M.J., Bolfarini, C. Surface chemical treatment of ultrafine-grained Ti-6Al-7Nb alloy processed by severer plastic deformation. *Journal of Alloys and Compounds* **643** (2015), 241-245.

[15] Chlebus, E., Kuznicka, B., Kurzynowski, T., Dybala. B. Microstructure and mechanical behavior of Ti-6Al-7Nb alloy produced by selective laser melting. *Material Characterization* **62** (2013), 488-495.

[16] Huang, H., Wu, C., Sun, Y., Yang, W., Lee. T. Surface nanotopography of an anodized Ti-6Al-7Nb alloy enhances cell growth. *Journal of Alloys and Compounds* **615** (2014), S648-S654.

[17] Rafieerad, A.R., Bushroa, A.R., Nasiri-Tabrizi, B., Vadivelu, J., Baradaran, S., Mesbah, M., Zavareh A. M. Mechanical properties, corrosion behavior and in-vitro bioactivity of

nanostructured Pd/ PdO coating on Ti-6Al-7Nb implant. *Materials and Design* **103** (2016), 10-24.

[18] Yamaguchi, M., Suzuki, S., Sasaki, S., Chiba, T., Itoh, N., Hoga. M. Fabrication of nano-periodic structures and modification of the Wenzel model to estimate contact angle. *Sensors and Actuators A: Physical* **212** (2014), 87-92.

[19] Han, T., Shr, J., Wu, C., Hsieh., C. A modified Wenzel model for hydrophobic behaviour of nanostructured surfaces. *Thin Solid Films* **515** (2017), 4666-4669.

[20] Kwok, S.Y., Li, D., Neumann. A.W., Fowkes. Surface tension component approach revisited. *Colloids and Surfaces A: Physicochemical and Engineering Aspects* **89** (1994), 181-191.

[21] Spelt, J.K., Neumann. A. W. Solid surface tension: the equation of state approach and the theory of surface tension components. Theoretical and conceptual considerations. *Langmuir* **3** (1987), 588-591.

[22] Robert D. A., Neumann, W. Contact angle patterns on Low-Energy surfaces. *Advances in Colloid and Interface Science* **206** (2014), 46-56.

[23] Cansoy, C.E., Erbil, H.Y., Orhan A., Tayfun A. Effect of pattern size and geometry on the use of Cassie-Baxter equation for surperhydrophobic surfaces. *Colloids and surfaces A: Physicochemical and Engineering Aspects* **386** (2011), 116-124.

[24] Ugur C., Cansoy. C. E. Applicability of Cassie-Baxter equation for superhydrophobic fluoropolymer-silica composite films. *Applied Surface Science* **335** (2015), 99-06.

[25] Jothi Prakash, C.G., Clement Raj, C. Prasanth, R. Fabrication of zero contact angle ultra-super hydrophilic surfaces. *Journal of Colloid and Interface Science* **496** (2017), 300-310.

[26] Thayawat U., Suwit S., Chotika V., Viboon T.. Laser cleaning performance and PAHs formation in the removal of roasting marinade stain. Food and Bioproducts Processing **102** (2017), 81-89.

[27] Jin, W., Wu, G., Feng, H., Wang, W., Zhang, X., Chu, P.K. Improvement of corrosion resistance and biocompatibility of rare-earth WE43 magnesium alloy by neodymium self-ion implantation. *Corrosion Science* **94** (2015), 142-155.